Drug Delivery and Translational Research (2023) 13:852–861
https://doi.org/10.1007/s13346-022-01249-9

ORIGINAL ARTICLE

Engineering of tetanus toxoid-loaded polymeric microneedle patches

Muhammad Sohail Arshad[1] · Shafaq Gulfam[1] · Saman Zafar[1] · Najmusama Abdul Jalil[2] · Nadia Ahmad[2] · Omar Qutachi[2] · Ming-Wei Chang[3] · Neenu Singh[4] · Zeeshan Ahmad[2]

Accepted: 3 October 2022 / Published online: 17 October 2022

Abstract

This study is aimed to fabricate tetanus toxoid laden microneedle patches by using a polymeric blend comprising of polyvinyl pyrrolidone and sodium carboxymethyl cellulose as base materials and sorbitol as a plasticizer. The tetanus toxoid was mixed with polymeric blend and patches were prepared by using vacuum micromolding technique. Microneedle patches were evaluated for physical attributes such as uniformity of thickness, folding endurance, and swelling profile. Morphological features were assessed by optical and scanning electron microscopy. In vitro performance of fabricated patches was studied by using bicinchoninic acid assay (BCA). Insertion ability of microstructures was studied in vitro on model skin parafilm and in vivo in albino rat. In vivo immunogenic activity of the formulation was assessed by recording immunoglobulin G (IgG) levels, interferon gamma (IFN-γ) levels, and T-cell ($CD4^+$ and $CD8^+$) count following the application of dosage forms. Prepared patches, displaying sharp-tipped and smooth-surfaced microstructures, remained intact after 350 ± 36 foldings. Optimized microneedle patch formulation showed ~ 74% swelling and ~ 85.6% vaccine release within an hour. The microneedles successfully pierced parafilm. Histological examination of microneedle-treated rat skin confirmed disruption of epidermis without damaging the underneath vasculature. A significant increase in IgG levels (~ 21%), IFN-γ levels (~ 30%), $CD4^+$ (~ 41.5%), and $CD8^+$ (~ 48.5%) cell count was observed in tetanus vaccine-loaded microneedle patches treated albino rats with respect to control (untreated) group at 42nd day of immunization. In conclusion, tetanus toxoid-loaded microneedle patches can be considered as an efficient choice for transdermal delivery of vaccine without inducing pain commonly experienced with hypodermic needles.

Keywords Tetanus toxoid vaccine · Microneedles · Polyvinyl pyrrolidone · Carboxymethyl cellulose · Bicinchoninic acid assay · Immunization · Flow cytometry · Interferon gamma · Immunoglobulin G

Introduction

Majority vaccines are administered via the conventional parenteral route which poses several limitations such as pain due to needle pricking of skin, risk of infection (e.g., bloodborne) transmission as a result of unsafe injection practices, requirement of trained personnel, and production of biohazardous waste [1–5]. During recent years, transdermal route has been widely used to overcome these limitations [6–12]. Moreover, an organized immune network comprising of high density of antigen-presenting and immune-accessory cells is present within the skin microenvironment. This makes skin an efficient immune responsive site, hence, a feasible target for vaccines delivery [13]. However, conventional transdermal patches are unable to efficiently administer high molecular weight vaccines (> 500 Daltons) across skin layers due to the barrier function of the stratum corneum. Several advanced methods have been used for transdermal administration of vaccines including iontophoresis (e.g., hepatitis B [14] and anticancer gp-100 peptide KVPRNQDWL vaccine [15]), electroporation (e.g., hepatitis C [16], influenza [17], and malaria [18] vaccine), and sonophoresis (tetanus toxoid [19] and hepatitis B [20] vaccine) employing electric impulse and acoustic waves, respectively. These approaches

✉ Zeeshan Ahmad
zahmad@dmu.ac.uk

1 Faculty of Pharmacy, Bahauddin Zakariya University, Multan, Pakistan

2 Leicester School of Pharmacy, De Montfort University, Leicester, UK

3 Nanotechnology and Integrated Bioengineering Centre, University of Ulster, Newtownabbey, Northern Ireland, UK

4 Leicester School of Allied Health Sciences, De Montfort University, Leicester, UK

seldom permit self-application of the medicament; a need for trained personnel for drug administration adds to the health care costs [21–23].

More recently, microneedle (MN) patches have emerged as promising candidates that breach the stratum corneum barrier in a minimally invasive manner and deliver large molecular weight therapeutic entities such as vaccines directly into the general circulation [24]. Literature reports suggest that the channels generated in the skin by MNs (of varying geometry, e.g., size 500 µm, 750 µm, and 1500 µm) gradually shrink followed by complete closure within ~ 3–40 h [25]. MN patches have been manufactured by using numerous materials, for example, metals, silicon, ceramics, glass, and polymers. Metal microneedles exhibit high tensile strength; however, these are not eco-friendly and produce hazardous waste. Silicon, ceramics, and glass MNs are brittle, hence, can easily break upon insertion into skin. Remnants of these materials in the skin can potentially lead to an injury. Polymers are considered as a suitable choice for MN fabrication due to their biocompatible, biodegradable, and non-toxic nature. Furthermore, modulated release and stimuli responsive delivery of drugs can also be achieved by using polymeric materials [22, 24, 26]. Over time, several vaccines including BCG, rabies, influenza, diphtheria, malaria, measles, rubella, polio, and COVID-19 have been successfully delivered by using MN patches prepared with numerous natural (e.g., hyaluronic acid, alginate, chitosan) and synthetic (e.g., polyvinyl alcohol, polyvinyl pyrrolidone, carboxymethyl cellulose) polymers [13, 21, 27–32].

Polyvinyl pyrrolidone (PVP) and sodium carboxymethyl cellulose (CMC) have been extensively employed for fabricating dissolving MNs. These polymers are preferred in the formulation due to their hydrophilicity, biocompatibility, biodegradability, inertness, and ability to protect loaded therapeutic moiety from denaturation [33–35]. Moreover, sodium CMC exhibits an adjuvant effect on immune responses induced by DNA vaccine formulations, hence, is intended as an efficient carrier for vaccines [36]. Following entry to general circulation, PVP accumulates in mesenteric lymph nodes [37]. PVP is reported to pass through post glomeruli capillaries. Moreover, disposition of PVP through reticuloendothelial system has also been reported [38]. CMC completely absorbs in the body. The mechanisms involve in the metabolism of CMC include hydrolysis of main polymeric chain and macrophagal pinocytosis. The products of CMC metabolism are completely eliminated (from the body) with the urine and feces without accumulation [39]. Sorbitol, a hydroxyl group-rich sugar, is employed as a plasticizer; can increase the flexibility; and reduce the brittleness of MN device [40].

The present study aims to fabricate tetanus vaccine-loaded MN patches by using PVP and sodium CMC blend as the MN base and sorbitol as a plasticizer. Prepared formulations were evaluated for in vitro release profile and in vivo immune response in albino rats.

Material and methods

Materials

Polyvinyl pyrrolidone (K30, molecular weight ~ 40,000 Da), sodium carboxy methyl cellulose (molecular weight ~ 25,000 Da), and D-sorbitol were purchased from Sigma Aldrich, St. Louis, Missouri, USA. Potassium di-hydrogen phosphate and disodium hydrogen phosphate were purchased from Duksan, Ansan, South Korea. Tetanus vaccine was purchased from Amson Vaccine & Pharma Pvt Ltd., Islamabad, Pakistan. BCA (bicinchoninic acid) assay kit was purchased from Thermo Fischer, Massachusetts, USA. Distilled water was obtained from in-house facility.

Preparation of microneedles

Polydimethylsiloxane (PDMS) silicon moulds of pre-determined MN sizes were fabricated by using stainless steel master molds following a procedure reported earlier by the authors [21, 26, 41]. Briefly, conventional machining procedures comprising of grinding, electro-discharge process, and electropolishing of the MNs were employed to manufacture stainless steel master molds. Liquid silicon solution was formulated by blending hardener (1 part) and Dow corning sylgard 184 silicon (9 parts). The prepared mixture was added in stainless steel master molds and heated at ~ 80 °C for 60 min. Cured PDMS silicon MN molds were separated from stainless steel master molds.

Aqueous solutions comprising of varying concentrations of PVP (20–37.5% w/v), sodium CMC (0.75–4% w/v), and sorbitol (15–20% w.r.t total solid polymeric weight) were prepared. Sodium CMC solutions were prepared in distilled water at 60 °C with continuous stirring for 1 h (solution I). PVP and sorbitol were dissolved in specified concentrations in distilled water to form a solution (solution II). Both the solutions were mixed and introduced to PDMS molds having needle shaped microcavities of sizes, i.e., 150 µm, 300 µm, and 500 µm, under vacuum [42]. Molds were subsequently incubated at room temperature for 48–72 h in a chamber containing silica desiccants. Upon drying, patches were removed from PDMS moulds and stored in air tight containers with silica desiccants till further use. For fabricating vaccine-loaded MN patch device, tetanus toxoid vaccine solution (50 µl for one patch with a thickness and width of 0.82 ± 0.010 mm and 7.91 ± 0.150 mm, respectively) was thoroughly mixed in the polymeric blend with continuous stirring at 300 rpm for 3–5 min. Vaccine-incorporated

patches were fabricated following the procedure mentioned earlier for blank MN formulations.

Physical evaluation

Optical imaging

The integrity of dry MN patches was studied by analyzing the images recorded with an HD camera, Samsung ES95, Seoul, South Korea, coupled with an optical microscope (Labomed, Los Angeles, USA) by using a 4× lens.

Uniformity of thickness and width

Thickness uniformity and width of patches ($N = 10$) were determined with the help of a vernier caliper (Lufen 02–067-4, Zhejiang, China) at six different points and mean ± standard deviation was calculated.

Folding endurance

Endurance and strength of prepared formulations ($N = 10$) were estimated by continuously folding the patch at the same point until a crack appeared on its surface.

Swelling study

Dried blank patches ($N = 5$) of known mass (W_0) were immersed, individually, for 2 min in a petri dish containing distilled water. The patches were taken out of petri dish, excess water was wiped off by filter paper, and the swollen polymeric devices were weighed (W_1). Percentage swelling was calculated by using the following formula.

$$Percentage\ swelling = \frac{W_1 - W_0}{W_0} \times 100$$

Scanning electron microscopy

Vaccine laden MN patches were studied for morphological attributes by using a scanning electron microscope (SEM). Formulations were sputtered coated (to ~ 10-nm thickness) with gold solution; micrographs were captured by field emission scanning electron microscope (Zeiss, Gemini SEM 300, Oberkochen, Germany) and examined for determining MN dimensions and morphology.

In vitro release study

For quantification of vaccine in the prepared MN patches, BCA protein assay kit was used which comprises bovine serum albumin (BSA) as standard protein and a bicinchoninic acid-based working reagent. A stock solution of BSA standard (250 µg/ml) was prepared. Different dilutions of stock solution namely 125, 50, 25, and 5 µg/ml were prepared and aliquots (200 µl) from each dilution were mixed with 4 ml of reagent. Following an incubation at 37 °C for 30 min, the absorbance of these samples was recorded at λ_{max} 562 nm by using a UV–visible spectrophotometer (Hitachi, U-1800, Tokyo Japan) and a calibration curve was constructed.

In vitro release study was performed in phosphate buffer (pH 5.5, 25 ml) at 300 rpm and 37 ± 2 °C. Tetanus toxoid-loaded MN patch was added in the dissolution medium; aliquots of 200 µl were drawn at specified intervals; 5,10, 20, 30, 40, 60, 90, and 120 min; and an equal volume of buffer was added to maintain sink conditions [43]. Each sample (200 µl) was mixed with working reagent (4 ml) and absorbance was recorded by following the procedure described above. The experiment was performed in triplicate. Tetanus toxoid protein content in the MN patch formulation was estimated by using calibration curve data. Different models (i.e., Higuchi, first order, zero order, and Korsmeyer-Peppas) were fitted to the obtained data in order to assess the release kinetics.

In vitro insertion study

Penetration ability of MNs was evaluated by using parafilm as a skin simulant [44]. The optimized MN device was applied on the film (thickness 125 µm, dimension 20 × 20 mm) by pressing with a thumb for 40–50 s. The imprints of needles on the flexible film were examined under an optical microscope.

Immunogenicity study

Animal study was conducted after approval from the Ethical Committee of Bahauddin Zakariya University Multan (190/PEC/2021). Wistar albino rats, *Rattus norvegicus domestica* ($N = 20$) with an average weight of 80–100 g, were kept at room temperature (25 ± 3 °C), under a 12-h dark/light cycle and allowed free access to food and water 48 h before the experiments. The animals were divided into four groups. Group 1 (negative control) was not given any treatment. Groups 2 and 3 received blank and vaccine-laden MN patches (containing 50 µl vaccine), respectively on the shaved abdominal region. The MN patches were applied by thumb pressure for 40–50 s (equivalent to a force of 1–1.5 N). Group 4 (positive control) was intramuscularly injected with standard tetanus vaccine (50 µl). Groups 2, 3, and 4 received primary and booster doses at 0th day and 22nd day, respectively. The blood samples were taken from all animals ($N = 20$) by penetrating the retro-orbital plexus with the help of sterile hematocrit capillary tubes at 1st,

10th, 21st, 32nd, 42nd day, and centrifuged at 2500 rpm for 10–15 min to obtain serum for immunoglobulin G (IgG) ELISA (enzyme-linked immunosorbent assay). The samples drawn on 42nd day were evaluated for interferon gamma, CD4 + and CD8 + levels.

Immunoglobulin G (IgG) ELISA

Roche (Basel, Switzerland) mouse IgG ELISA kit was used to determine IgG antibodies in the samples. A 50 µl capture antibody (anti-mouse-Fcγ from sheep) solution, a 200 µl blocking reagent (consisting of gelatin, tris hydrochloride buffer, and sodium chloride) and 50-µl test sample were pipetted into a 96 wells microplate one by one and incubated for 90, 15 and 60 min, respectively. Upon completion of incubation period, each solution was discarded and wells were washed with a wash solution (prepared in distilled water by using tween 20 and sodium chloride). Then, a conjugate solution (comprising of anti-mouse-κ-POD [peroxidase] and anti-mouse-λ-POD from sheep) diluted with blocking reagent (1:20 v/v) was poured (50 µl) inside the wells and kept for 60 min. Solution removal and washing steps were repeated. A 50 µl substrate solution of 2,2′-azino-bis [3-ethylbenzothiazoline-6-sulphonic acid] was transferred into the wells and incubated for 60 min. The absorbance was recorded at 405 nm by using an ELISA plate reader (BioTek 800Ts Winooski, Vermont, United States) and total IgG levels were measured.

Interferon gamma (IFN-γ) ELISA

Interferon gamma (IFN-γ) levels were determined by mouse IFN-γ mouse ELISA kit (Abcam, Cambridge, UK). The procedure involved sequential addition of (i) primary capture antibody solution, (ii) IFN-γ standard and test samples, (iii) biotinylated IFN-γ detection antibody reagent, (iv) horseradish peroxidase-streptavidin solution, and (v) tetramethyl benzidine (TMB) substrate reagent into the wells of a microplate. Each solution/reagent (100 µl) was incubated for specified time (i.e., 90, 150, 60, 45, and 30 min, respectively). After incubation, the solutions were discarded and wells were washed with a wash solution (1% tween 20 in phosphate-buffered saline). A phosphoric acid comprising stop solution was immediately added after completion of TMB substrate reagent incubation period and absorbance was recorded at 450 nm by using a microplate reader.

Flow cytometry assay

The heparinized blood sample was diluted with physiological saline in 1:1. The mixture was loaded slowly (to avoid mixing of blood and medium) on the surface of a polysucrose and sodium diatrizoate-based lymphocyte separation medium (MP Biomedicals, Irvine, California, USA) resulting in the formation of a sharp blood-lymphocyte separation medium interface. The mixture was centrifuged at 2000 rpm for 15–20 min at 20 °C. Top plasma layer was discarded. The lymphocyte layer plus half of the lymphocyte separation medium layer below it was aspirated, diluted with an equal amount of buffered balanced salt solution, and centrifuged at 500 rpm for 10 min at 20 °C. The sedimented cells were collected and washed twice by using buffered balanced salt solution.

The collected cells were suspended in the flow buffer comprising of phosphate-buffered saline, fetal calf serum, and sodium azide. Fluorescein isothiocyanate conjugated $CD4^+$ and $CD8^+$ monoclonal antibodies (BioLegend, San Diego, California, USA) were added to the cell suspension. The solutions were incubated for 30 min at 20 °C in dark. Subsequently, cells were washed and centrifuged at 2000 rpm for 5 min in the flow buffer twice to remove unbound antibodies. The cells were resuspended in the flow buffer, analyzed on the flow cytometer (BD Biosciences, Franklin Lakes, New Jersey, USA), and T-cells ($CD4^+$ and $CD8^+$) were counted [45, 46].

Histological examination

After completion of in vivo study, a MN patch-treated animal was sacrificed and micropierced skin was excised by using a sterile blade. The excised skin was fixed in 37% formaldehyde. Microtome was used to cut skin specimen into thin (~ 1–2 µm) slices followed by fixation (on a glass slide) and hematoxylin and eosin (H&E) staining. The stained skin was examined under an optical microscope (Labomed, Los Angeles, USA) to observe the changes in skin following needle penetration and results were compared with the untreated counterpart.

Results

Physical evaluation

The results from the preliminary examination of MN formulations are represented in Table 1. Polymeric solutions comprising of low concentration of sodium CMC (i.e., 0.75–2.5% w/v) and PVP (i.e., 20% w/v) were dilute and formed brittle MN patches. The polymeric solutions comprising of high concentration of sodium CMC (i.e., 4% w/v) formed thick gels and were difficult to pour in the PDMS molds. MN patch formulations comprising of intermediate concentration, i.e., sodium CMC 3% w/v and PVP 25% w/v concentration exhibited appropriate microstructure and satisfactory folding endurance. In the case of plasticizer, patches containing 20% (w.r.t total dry polymeric mass) sorbitol

Table 1 Physical evaluation of MN patch formulations

Formulation code and composition	Thickness (mm)	Width (mm)	Folding endurance	Swelling (%)	MN morphology/ integrity
F_1 (sodium CMC 0.75%, PVP 37.5%, sorbitol 15%)	0.82 ± 0.011	8.10 ± 0.089	0 ± 0	–-	+
F_2 (sodium CMC 1%, PVP 25%, sorbitol 15%)	0.80 ± 0.02	7.96 ± 0.121	10 ± 3	–-	+
F_3 (sodium CMC 2%, PVP 25%, sorbitol 15%)	0.80 ± 0.016	7.89 ± 0.102	12 ± 2	–-	+
F_4 (sodium CMC 2%, PVP 25%, Sorbitol 20%)	0.80 ± 0.012	7.91 ± 0.162	100 ± 18	69.8 ± 0.034	+ + +
F_5 (sodium CMC 2.5%, PVP 25%, sorbitol 15%)	0.81 ± 0.015	7.91 ± 0.141	350 ± 42	22.44 ± 0.009	+ + +
F_6 (sodium CMC 4%, PVP 20%, sorbitol 15%)	0.80 ± 0.011	7.91 ± 0.132	500 ± 39	18.57 ± 0.009	+ + +
F_7 (sodium CMC 4%, PVP 25%, sorbitol 15%)	0.80 ± 0.012	7.91 ± 0.140	500 ± 45	7.95 ± 0.005	+ +
F_8 (sodium CMC 4%, PVP 30%, sorbitol 15%)	0.80 ± 0.013	7.91 ± 0.122	500 ± 21	68 ± 0.060	+ + +
F_9 (sodium CMC 3%, PVP 25%, sorbitol 15%)	0.81 ± 0.013	7.89 ± 0.171	400 ± 53	72 ± 0.029	+ + + +
F_{10} (sodium CMC 3%, PVP 25%, sorbitol 15%, 50 µl tetanus vaccine)	0.82 ± 0.010	7.91 ± 0.150	350 ± 36	74 ± 0.026	+ + + +

The symbol + + + + means good; + + + means average; + + means poor; + means very poor

were found to be malleable. Hence, the optimized MN patch formulation comprising of 25% w/v PVP, 3% w/v sodium CMC, and 15% (w.r.t total dry weight of base materials) sorbitol was selected for further evaluation.

Prepared MN patches were found to be light yellow in color (Fig. 1 left) with a reproducible average thickness and width of ~ 0.82 ± 0.010 mm and 7.91 ± 0.150 mm, respectively. Photographic images confirmed an even distribution of microstructures (Fig. 1 right). The optimized patch did not exhibit any cracks or loss of integrity after folding for 350 ± 36 times indicating that formulated device would withstand mechanical stresses which are experienced during shipment and application. The patches showed a swelling of 74 ± 0.026% allowing rapid uptake of physiological fluids and release of incorporated vaccine.

Scanning electron microscopy

The SEM images confirmed the presence of evenly distributed needles displaying pointed and sharp tips (Fig. 2). The microstructures exhibited smooth and uniform surface without any irregularity. The tiny needles with sharp tips and appropriate height are expected to efficiently deliver incorporated vaccine in the general circulation without stimulating the pain receptors.

In vitro release study

During the in vitro release study, 18.4 ± 2.1% vaccine was released from the MN device (F_{10}) within the first 5 min. Over the next 25 min, another ~ 43 ± 3.2% vaccine release was observed. Within 60 min, ~ 85.6 ± 2.9% vaccine was released from the prepared patch (Fig. 3 bottom). On the basis of *R*-square value, the dissolution modeling confirmed that the vaccine release profile followed first-order kinetics.

In vitro insertion study

Microscopic photographs (Fig. 4) of parafilm showed evidence of needle penetration. Complementary structure of

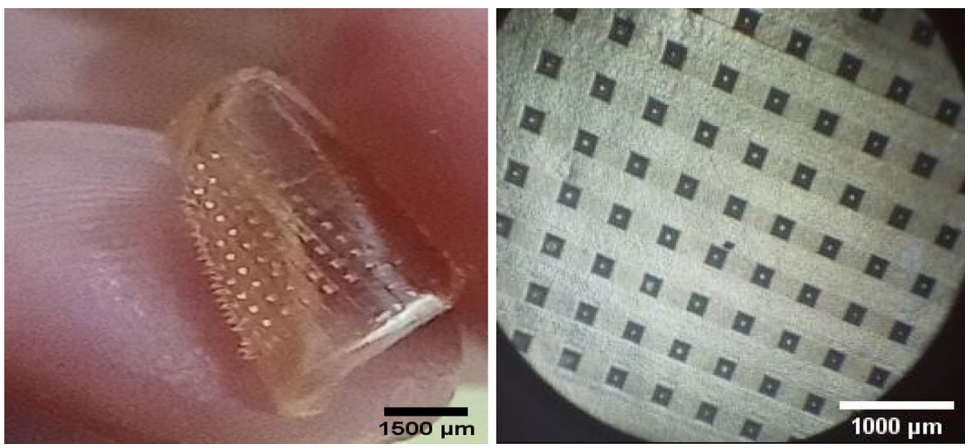

Fig. 1 (Left) Photographic image of MN device, (right) needles of size 300 µm under optical microscope

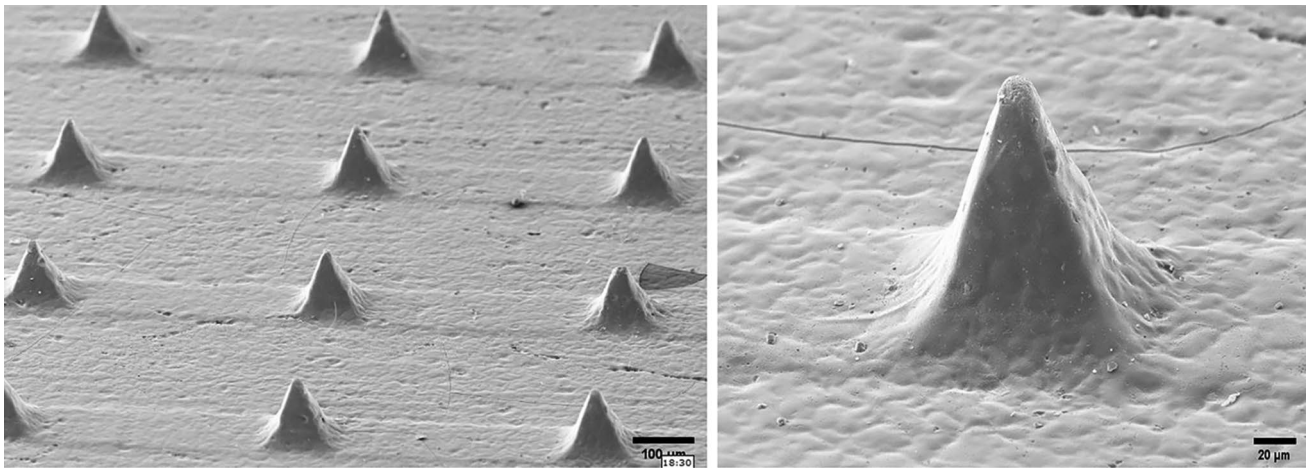

Fig. 2 SEM photomicrographs of MNs

MNs was successfully reproduced on the skin simulant parafilm. Clear imprints of microstructures (size ≥ 300 µm) on the parafilm suggested that the prepared device would efficiently breach the skin barrier and deliver the incorporated drug to the general circulation.

Immunogenicity study

Immunoglobulin G ELISA

The control group showed IgG levels of 1.07 g/l. On the 21st day of immunization, IgG levels exhibited by blank MN patch, vaccine-laden MN patch, and standard intramuscular injection treated rats were1.0 ± 0.07 g/l, 1.20 ± 0.04 g/l, and 1.30 ± 0.05 g/l, respectively. A slight increase, i.e., 1.23 ± 0.07 g/l and 1.34 ± 0.04 g/l in IgG levels of group 3 and 4, respectively was observed on the 32nd day. Highest IgG levels were displayed by these groups on 42nd day. A ~ 21.3% and ~ 32.5% increase in antibody levels was recorded in rats treated with vaccine laden MN patches (1.31 ± 0.05 g/l) and intramuscular injection (1.43 ± 0.08 g/l) with respect to control group (Fig. 5). The prepared MN patch formulation successfully induced humoral immunity and the results are comparable with the standard intramuscular injection.

Interferon gamma ELISA

IFN-γ levels shown by control, blank MN device, tetanus vaccine-loaded MN patch, and standard intramuscular injection administered groups were 21.91 ± 1.1 ng/l, 22.83 ± 1.5 ng/l, 28.54 ± 2.2 ng/l, and 38.28 ± 1.8 ng/l, respectively (Fig. 6). A significant increase, i.e., ~ 30% in IFN-γ levels of MN patch-treated group as compared to the control group suggested an induction of immune response following administration of vaccine.

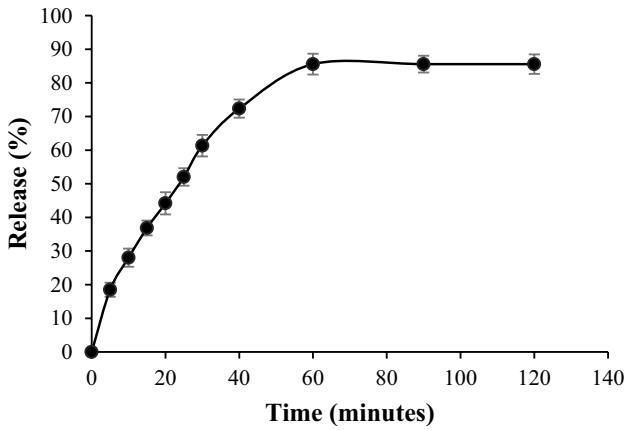

Fig. 3 In vitro release profile of vaccine from MN patch

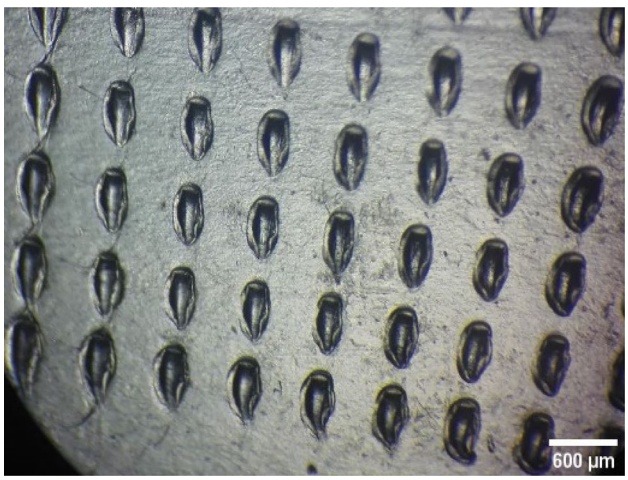

Fig. 4 Microscopic image of MNs on simulated skin

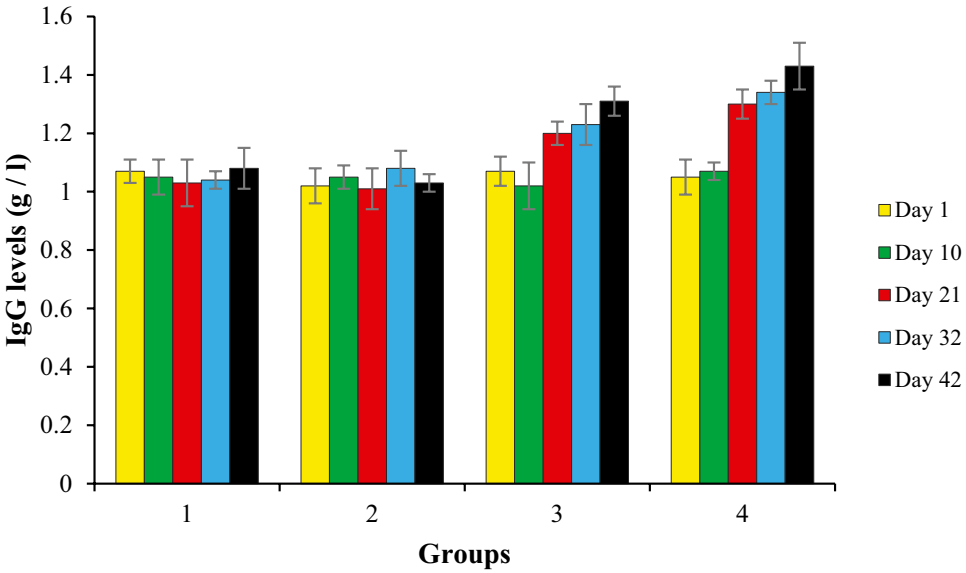

Fig. 5 IgG levels measured over different time intervals for all groups

Flow cytometry assay

$CD4^+$ count observed in group 1 and 2 was $2618 \pm 120/mm^3$ and $2550 \pm 100/mm^3$, respectively. A significant increase in absolute count of $CD4^+$ cells was observed in vaccine-loaded MN device-treated group ($3704 \pm 90/mm^3$) and results were comparable with standard intramuscular injection administered group, i.e., $3918 \pm 115/mm^3$ (Fig. 7 top).

$CD8^+$ cell levels recorded in the control group and blank MN patch-treated group were $1941 \pm 100/mm^3$ and $1990 \pm 115/mm^3$, respectively. $CD8^+$ cell levels were elevated in the vaccine-loaded MN device-treated group ($2881 \pm 85/mm^3$). The $CD8^+$ cell count was $3134 \pm 112/mm^3$ in standard intramuscular injection given group (Fig. 7 bottom). These results suggest that the prepared MN patches are capable of inducing T-cell-mediated immunity.

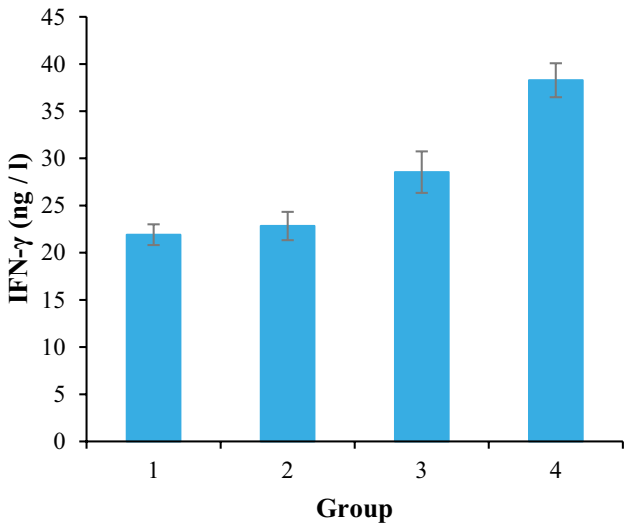

Fig. 6 Interferon gamma levels exhibited by all group

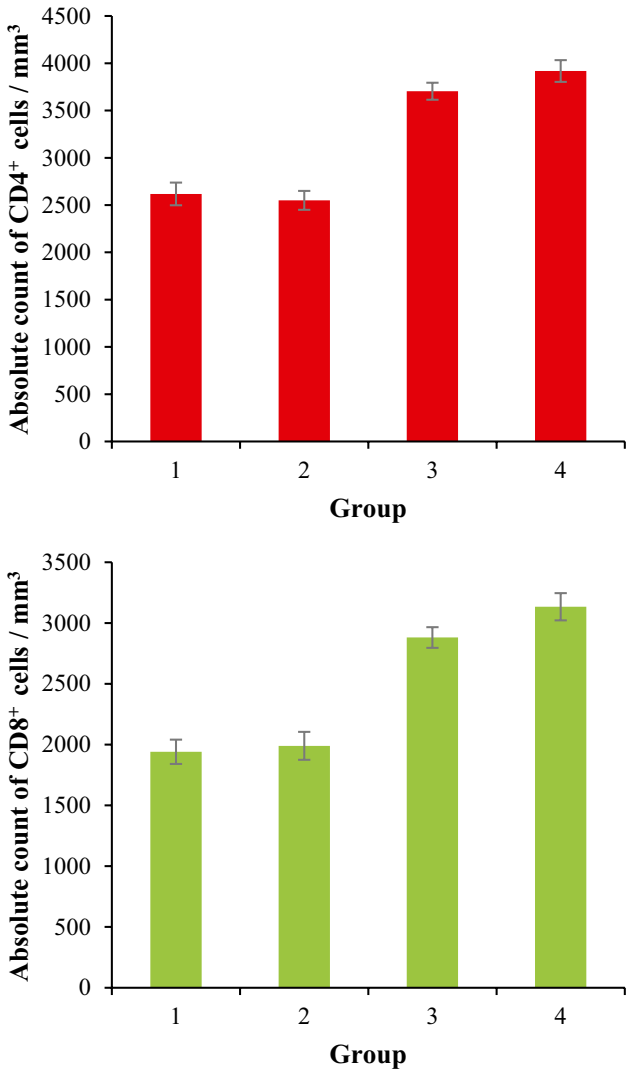

Fig. 7 $CD4^+$ (top) and $CD8^+$ (bottom) absolute count exhibited by all group

Histological examination

Microscopic images of H&E-stained control and MN-treated skin samples are represented in Fig. 8. The outermost skin layer epidermis was intact in control skin sample while MN-treated skin exhibited a disrupted epidermis and invasions were clearly visible at several points. Dermis, connective tissue, and blood vessels remained intact in MN-treated skin, hence, suggesting that prepared MNs did not damage deep skin structures and pierced the skin in a minimally invasive manner.

Discussion

Tetanus is a common infection in low- and middle-income countries. In 2015, ~ 79% of the deaths recorded worldwide due to tetanus occurred in south Asia and sub-Saharan Africa. In the same year, neonatal tetanus (infection occurring within 28 days of birth) resulted in ~ 34,000 deaths. Although there has been a decline in the incidence rate of tetanus in the developing countries, the mortality rate, particularly for patients aged over 60 years, is > 50%. The incidence of tetanus infection surge in natural disasters due to the lack of resources (e.g., vaccine supply and health personnel) in these situations. At the same time, a higher number of tetanus-prone injuries are observed which in combination with the geographic displacement of the population further worsen the public health. For instance, in Aceh, Indonesia and Kashmir, Pakistan, 106 and 139 tetanus cases were reported in the months following tsunami in 2004 and earthquake 2005, respectively. Although tetanus is a vaccine-preventable infection [47], administration of vaccine via the invasive parenteral route requires trained personnel (which raises the overall cost of vaccine by 25%) and bruised patients are frequently left non-compliant. Transdermal route seldom serves as an alternate as high molecular weight vaccines cannot pass through the intact stratum corneum due to its barrier function [48].

Recently, MNs emerged as potential contenders for transdermal vaccine administration due to their ability to breach the stratum corneum and deliver vaccines into the systemic circulation without stimulating nociceptors [49]. Moreover, MNs are self-administrable, hence, can offer convenient and quick immunization during natural disasters and in resource-poor countries.

In this study, polymeric dissolvable MN patches were prepared with PVP and sodium CMC (as microarray base) and sorbitol (as plasticizer) by using the vacuum micromolding approach. Optimized MN patches were successfully folded for 350 ± 36 times suggesting integrity of preparation. SEM and optical microscopy results confirmed presence of equidistant microstructures with uniform surface and pointed and sharp tips. Imprints of tiny needles on the model skin parafilm confirmed the penetration ability of optimized MN formulation. The prepared device successfully breached the stratum corneum during in vivo insertion study on albino rats without damaging deep skin structures. A swelling percentage of ~ 74% indicated ability of prepared polymeric formulation to efficiently uptake the liquid and rapidly release encapsulated vaccine. These tendencies are validated in in vitro studies wherein ~ 85.6% of the drug was

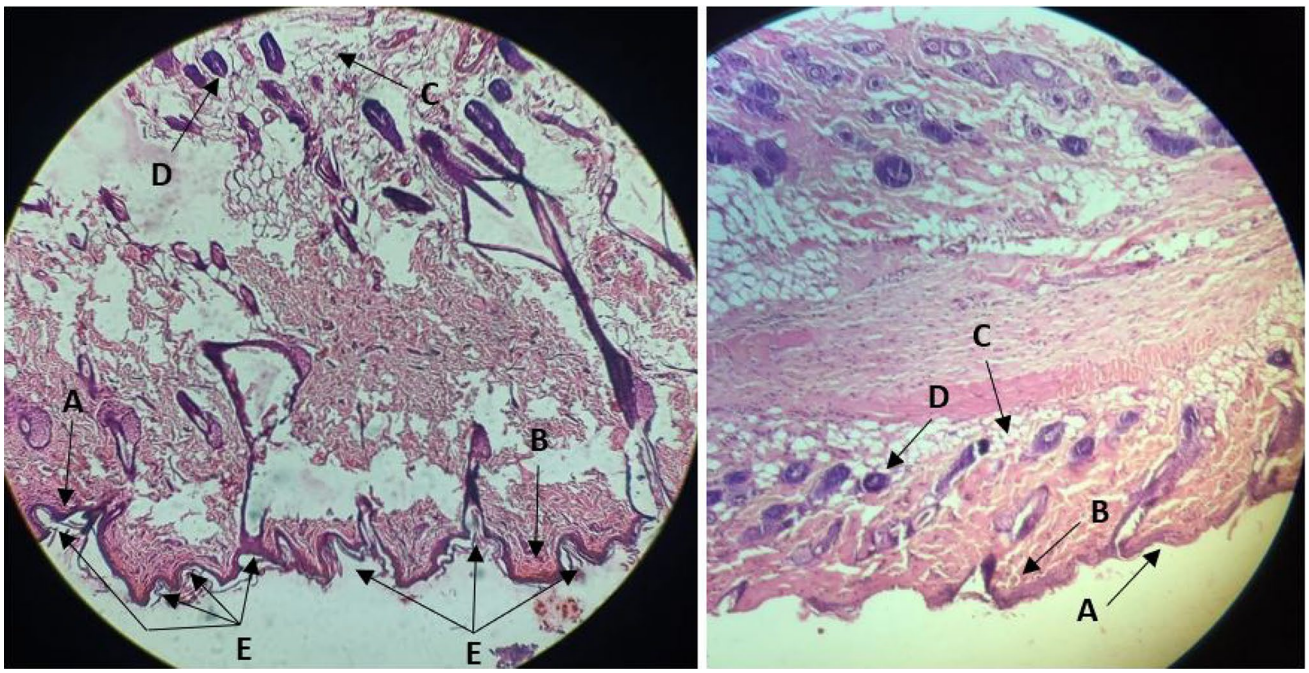

Fig. 8 Microscopic images of MN device-treated (left) and control (right) rat skin (**A** epidermis, **B** dermis, **C** connective tissue, **D** blood vessels, **E** disrupted epidermis)

released within an hour. During in vivo study in rats, IgG levels were increased by ~ 21% following MN application (1.31 ± 0.05 g/l) w.r.t control (1.08 ± 0.07 g/l) indicating the production of humoral response. IFN-γ levels also soared by ~ 30% in MN patch applied rats (28.54 ± 2.2 ng/l) of the control (21.91 ± 1.1 ng/l). A significant increase in IFN-γ levels denotes activation of macrophages, natural killer cells and neutrophils. A ~ 41.5% and ~ 48.5% increase in $CD4^+$ and $CD8^+$ cell count, respectively, following the application of MN formulation suggested generation of T-cell response. It is noteworthy that the immune responses in tetanus toxoid MN patch-treated animals were comparable to the counterparts treated with intramuscular injections. The MN patch formulation approach can be considered as an attractive alternative to the conventional intramuscular injection as this is minimally invasive and self-applicable in nature, thus, promising an improved patient compliance and reduced healthcare cost especially in resource-poor settings.

Conclusion

Tetanus toxoid encapsulated microneedle patches of acceptable microstructure, i.e., evenly positioned microstructures with pointed tips and uniform surface were prepared by using polyvinyl pyrrolidone, sodium carboxymethyl cellulose, and sorbitol. Histological examination of microneedle-treated rat skin confirmed disruptions in the outer layer of epidermis without damaging the deeper tissues containing nociceptors. Following administration of microneedle patch, an increase in immunoglobulin G levels (~ 21%), interferon gamma levels (~ 30%), and $CD4^+$ (~ 41.5%) and $CD8^+$ (~ 48.5%) cell count in treated albino rats suggested an induction of humoral and T-cell-mediated immunity (comparable to intramuscular injection) as well as activation of macrophages, neutrophils, and natural killer cells. It was therefore concluded that prepared microneedle patch formulation can serve as a promising candidate for transcutaneous immunization especially in resource-poor settings due to self-applicating and minimally invasive nature.

Author contribution Muhammad Sohail Arshad: conceptualization and supervision; Shafaq Gulfam: experimentation and data analysis; Saman Zafar: data analysis and manuscript writing; Najmusama Abdul Jalil: data analysis, manuscript writing and review; Nadia Ahmad: data analysis, manuscript writing and review; Ming-Wei Chang: data analysis, manuscript writing and review; Neenu Singh: data analysis, manuscript writing and review; Zeeshan Ahmad: conceptualization and supervision.

Funding The authors acknowledge the financial support provided by the Higher Education Commission of Pakistan under National Research Program for Universities (NRPU) vide No. 7401/Punjab/NRPU/R&D/HEC/2017.

Data availability All data are made available with the article.

Declarations

Ethical approval and consent to participate Animal study was conducted after approval from the Ethical Committee of Bahauddin Zakariya University Multan (190/PEC/2021).

Consent for publication Yes.

Competing interests The authors declare no competing interests.

References

1. Zafar S, Arshad MS, Fatima S, Ali A, Zaman A, Sayed E, et al. COVID-19: Current developments and further opportunities in drug delivery and therapeutics. Pharmaceutics. 2020;12:1–25.
2. Arshad MS, Zafar S, Yousef B, Alyassin Y, Ali R, AlAsiri A, et al. A review of emerging technologies enabling improved solid oral dosage form manufacturing and processing. Adv Drug Deliv Rev. 2021;113840.
3. Yunos DM, Ahmad Z, Boccaccini AR. Fabrication and characterization of electrospun poly-DL-lactide (PDLLA) fibrous coatings on 45S5 Bioglass® substrates for bone tissue engineering applications. J Chem Technol Biotechnol. 2010;85:768–74.
4. Wang JC, Chang MW, Ahmad Z, Li JS. Fabrication of patterned polymer-antibiotic composite fibers via electrohydrodynamic (EHD) printing. J Drug Deliv Sci Technol. 2016;35:114–23.
5. Toman P, Lien C-F, Ahmad Z, Dietrich S, Smith JR, An Q, et al. Nanoparticles of alkylglyceryl-dextran-graft-poly (lactic acid) for drug delivery to the brain: preparation and in vitro investigation. Acta Biomater. 2015;23:250–62.
6. Mehta P, Zaman A, Smith A, Rasekh M, Haj-Ahmad R, Arshad MS, et al. Broad scale and structure fabrication of healthcare materials for drug and emerging therapies via electrohydrodynamic techniques. Adv Ther. 2019;2:1800024.
7. Ali A, Zaman A, Sayed E, Evans D, Morgan S, Samwell C, et al. Electrohydrodynamic atomisation driven design and engineering of opportunistic particulate systems for applications in drug delivery, therapeutics and pharmaceutics. Adv Drug Deliv Rev. 2021;176: 113788.
8. Mehta P, Rasekh M, Patel M, Onaiwu E, Nazari K, Kucuk I, et al. Recent applications of electrical, centrifugal, and pressurised emerging technologies for fibrous structure engineering in drug delivery, regenerative medicine and theranostics. Adv Drug Deliv Rev. 2021;175: 113823.
9. Nazari K, Kontogiannidou E, Ahmad RH, Gratsani A, Rasekh M, Arshad MS, et al. Development and characterisation of cellulose based electrospun mats for buccal delivery of non-steroidal anti-inflammatory drug (NSAID). Eur J Pharm Sci. 2017;102:147–55.
10. Ahmad Z, Stride E, Edirisinghe M. Novel preparation of transdermal drug-delivery patches and functional wound healing materials. J Drug Target. 2009;17:724–9.
11. Gao Y, Chang M-W, Ahmad Z, Li J-S. Magnetic-responsive microparticles with customized porosity for drug delivery. Rsc Adv. 2016;6:88157–67.
12. Ahmad Z, Thian ES, Huang J, Edirisinghe MJ, Best SM, Jayasinghe SN, et al. Deposition of nano-hydroxyapatite particles utilising direct and transitional electrohydrodynamic processes. J Mater Sci Mater Med. 2008;19:3093–104.
13. Korkmaz E, Balmert SC, Sumpter TL, Carey CD, Erdos G, Falo LD Jr. Microarray patches enable the development of skin-targeted vaccines against COVID-19. Adv Drug Deliv Rev. 2021;171:164–86.

14. Xu T, Xu Y-H, Wei M-Y, Deng L-H, Wu C-B. In vitro study of transdermal penetration and iontophoresis of hepatitis B vaccines through rat skin. Acta Pharm Sin. 2011;46:713–9.
15. Toyoda M, Hama S, Ikeda Y, Nagasaki Y, Kogure K. Anti-cancer vaccination by transdermal delivery of antigen peptide-loaded nanogels via iontophoresis. Int J Pharm. 2015;483:110–4.
16. Ahlén G, Söderholm J, Tjelle T, Kjeken R, Frelin L, Höglund U, et al. In vivo electroporation enhances the immunogenicity of hepatitis C virus nonstructural 3/4A DNA by increased local DNA uptake, protein expression, inflammation, and infiltration of CD3+ T cells. J Immunol. 2007;179:4741–53.
17. Laddy DJ, Yan J, Khan AS, Andersen H, Cohn A, Greenhouse J, et al. Electroporation of synthetic DNA antigens offers protection in nonhuman primates challenged with highly pathogenic avian influenza virus. J Virol. 2009;83:4624–30.
18. LeBlanc R, Vasquez Y, Hannaman D, Kumar N. Markedly enhanced immunogenicity of a Pfs25 DNA-based malaria transmission-blocking vaccine by in vivo electroporation. Vaccine. 2008;26:185–92.
19. Polat BE, Blankschtein D, Langer R. Low-frequency sonophoresis: application to the transdermal delivery of macromolecules and hydrophilic drugs. Expert Opin Drug Deliv. 2010;7:1415–32.
20. Hu Y, Yang M, Huang H, Shen Y, Liu H, Chen X. Controlled ultrasound erosion for transdermal delivery and hepatitis B immunization. Ultrasound Med Biol. 2019;45:1208–20.
21. Arshad MS, Fatima S, Nazari K, Ali R, Farhan M, Muhammad SA, et al. Engineering and characterisation of BCG-loaded polymeric microneedles. J Drug Target. 2020;28:525–32.
22. Ali R, Mehta P, Arshad M, Kucuk I, Chang MW, Ahmad Z. Transdermal microneedles—A materials perspective. AAPS PharmSciTech. 2020;21:1–14.
23. Ahmad Z, Nangrejo M, Edirisinghe M, Stride E, Colombo P, Zhang HB. Engineering a material for biomedical applications with electric field assisted processing. Appl Phys A. 2009;97:31–7.
24. Haj-Ahmad R, Khan H, Arshad MS, Rasekh M, Hussain A, Walsh S, et al. Microneedle coating techniques for transdermal drug delivery. Pharmaceutics. 2015;7:486–502.
25. Gupta J, Gill HS, Andrews SN, Prausnitz MR. Kinetics of skin resealing after insertion of microneedles in human subjects. J Control Release. 2011;154:148–55.
26. Arshad MS, Zafar S, Zahra AT, Zaman MH, Akhtar A, Kucuk I, et al. Fabrication and characterisation of self-applicating heparin sodium microneedle patches. J Drug Target. 2021;29:60–8.
27. Laurent PE, Bourhy H, Fantino M, Alchas P, Mikszta JA. Safety and efficacy of novel dermal and epidermal microneedle delivery systems for rabies vaccination in healthy adults. Vaccine. 2010;28:5850–6.
28. Kim Y-C, Quan F-S, Yoo D-G, Compans RW, Kang S-M, Prausnitz MR. Improved influenza vaccination in the skin using vaccine coated microneedles. Vaccine. 2009;27:6932–8.
29. Matsuo K, Hirobe S, Yokota Y, Ayabe Y, Seto M, Quan Y-S, et al. Transcutaneous immunization using a dissolving microneedle array protects against tetanus, diphtheria, malaria, and influenza. J Control Release. 2012;160:495–501.
30. Prausnitz MR, Goodson JL, Rota PA, Orenstein WA. A microneedle patch for measles and rubella vaccination: a game changer for achieving elimination. Curr Opin Virol. 2020;41:68–76.
31. Edens C, Dybdahl-Sissoko NC, Weldon WC, Oberste MS, Prausnitz MR. Inactivated polio vaccination using a microneedle patch is immunogenic in the rhesus macaque. Vaccine. 2015;33:4683–90.
32. Kim E, Erdos G, Huang S, Kenniston TW, Balmert SC, Carey CD, et al. Microneedle array delivered recombinant coronavirus vaccines: immunogenicity and rapid translational development. EBioMedicine. 2020;55: 102743.
33. Rahman M, Hasan M, Nitai AS, Nam S, Karmakar AK, Ahsan M, et al. Recent Developments of Carboxymethyl Cellulose. Polymers (Basel). 2021;13:1–48.
34. Chen L, Zhou H, Hao L, Chen H, Zhou X. Soy protein isolate-carboxymethyl cellulose conjugates with pH sensitivity for sustained avermectin release. R Soc Open Sci. 2019;6: 190685.
35. Sun W, Araci Z, Inayathullah M, Manickam S, Zhang X, Bruce MA, et al. Polyvinylpyrrolidone microneedles enable delivery of intact proteins for diagnostic and therapeutic applications. Acta Biomater. 2013;9:7767–74.
36. Hamajima K, Sasaki S, Fukushima J, Kaneko T, Xin K-Q, Kudoh I, et al. Intranasal administration of HIV-DNA vaccine formulated with a polymer, carboxymethylcellulose, augments mucosal antibody production and cell-mediated immune response. Clin Immunol Immunopathol. 1998;88:205–10.
37. Kurakula M, Rao GSNK. Pharmaceutical assessment of polyvinylpyrrolidone (PVP): As excipient from conventional to controlled delivery systems with a spotlight on COVID-19 inhibition. J Drug Deliv Sci Technol. 2020;60: 102046.
38. Nair B. Final report on the safety assessment of polyvinylpyrrolidone (PVP). Int J Toxicol. 2016;17:95–130.
39. Turaev AS. Dependence of the biodegradability of carboxymethylcellulose on its supermolecular structure and molecular parameters. Chem Nat Compd. 1995;31:254–9.
40. Arshad MS, Zahra AT, Zafar S, Zaman H, Akhtar A, Ayaz MM, et al. Antibiofilm effects of macrolide loaded microneedle patches: prospects in healing infected wounds. Pharm Res. 2021;38:165–77.
41. Zafar S, Hassan S, Mudassir J, Hussain A, Abbas N, Latif S, et al. Microneedle based transcutaneous delivery of low molecular weight heparin. Pak J Pharm Sci. 2021;34:1165–70.
42. Arshad MS, Hassan S, Hussain A, Abbas N, Kucuk I, Nazari K, et al. Improved transdermal delivery of cetirizine hydrochloride using polymeric microneedles. DARU J Pharm Sci. 2019;27:673–81.
43. Sayed E, Karavasili C, Ruparelia K, Haj-Ahmad R, Charalambopoulou G, Steriotis T, et al. Electrosprayed mesoporous particles for improved aqueous solubility of a poorly water soluble anticancer agent: In vitro and ex vivo evaluation. J Control Release. 2018;278:142–55.
44. Larrañeta E, Moore J, Vicente-Pérez EM, González-Vázquez P, Lutton R, Woolfson AD, et al. A proposed model membrane and test method for microneedle insertion studies. Int J Pharm. 2014;472:65–73.
45. Barbesti S, Soldini L, Carcelain G, Guignet A, Colizzi V, Mantelli B, et al. A simplified flow cytometry method of CD4 and CD8 cell counting based on thermoresistant reagents: Implications for large scale monitoring of HIV-infected patients in resource-limited settings. Cytom Part B Clin Cytom. 2005;68:43–51.
46. Mura M, Chaudhury S, Farooq F, Duncan EH, Beck K, Bergmann-Leitner ES. Optimized flow cytometric protocol for the detection of functional subsets of low frequency antigen-specific CD4+ and CD8+ T cells. MethodsX. 2020;7: 101005.
47. Yen LM, Thwaites CL. Tetanus Lancet. 2019;393:1657–68.
48. Prausnitz MR, Langer R. Transdermal drug delivery. Nat Biotechnol. 2008;26:1261–8.
49. Bhatnagar S, Dave K, Venuganti VVK. Microneedles in the clinic. J Control Release. 2017;260:164–82.